Simulation of Buckling-Driven Crack Growth in Layered Materials

by
Karl-Fredrik Nilsson
The Aeronautical Research Institute of Sweden
Structures Department
P.O. Box 110 21, S-161 11 Bromma, Sweden

SUMMARY

A finite element method to simulate buckling driven delamination growth in general circumstances is presented. Crack grow is assumed to be governed by a critical value of the energy release rate or a mixed fracture mode criterion. The FE-method is extended with a method for automatic remeshing to account for a continuously changing front. The method is first exemplified by computing the shape of the delamination front and the associated load required to sustain growth for an isotropic material subjected to uniaxial compression but governed by different mixed mode criteria.

To assess the validity and applicability of the proposed method an embedded delamination in a carbon epoxy laminate loaded in compression is analysed in a combined numerical/experimental study. Predicted and observed results are compared as regards the postbuckling behaviour and in particular the shape of the delamination front and the load needed to drive the growth.

INTRODUCTION

The use of layered materials in various structures has in the past decade received increasing attention. Fibre-reinforced composites, frequently used in aerospace applications, is perhaps the most obvious example. Layered materials are, however, used in other applications of technical significance as well such as ceramic surface coatings or protective coatings on electronical devices. Common to all layered materials is that individual layers might separate from each other, a phenomenon called delamination. One of the most treacherous features of delaminations is that although very hard to detect by visual inspection, they might still very well impair the structural integrity or functioning. It is therefore imminent that theoretical and numerical methods in conjunction with decisive experiments to assess the criticality of delaminations in various situations are developed. Overviews on the issue can be found in Garg[1], Storåkers[2], Abrate[3] and Hutchinson and Suo[4].

The sequence of events for a layered material with a single delamination and loaded in compression such that the delamination starts to spread is illustrated in Fig. 1.

The problem in general situations is very complex: delaminations might have arbitrary shapes; nonlinear kinematics have to be considered; the material is often anisotropic and inhomogeneous; contact between delaminated members rather seems to be the rule; last but not the least the criterion for crack growth may be very complex.

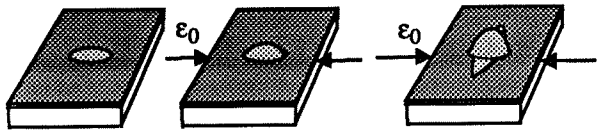

Fig. 1 Sequence of events at delamination buckling and growth. a) Unloaded cracked panel. b) Buckling and postbuckling of delaminated member. c) Delamination growth.

Referring to Fig. 1, it seems logical to deal with the delamination problem by a combination of structural analysis and fracture mechanics. The earliest attempts in this spirit by Kachanov[5], Chai and Babcock[6] and Yin[7] were based on a one-dimensional or axi-symmetrical analysis, i.e. the shape of the delamination could be described by one parameter prior to, as well as after, growth and with the total energy release rate as the crack driving force. These models have the virtue that the problem may be solved by analytical means or by relatively simple numerical methods which allows us to establish a basic understanding of the phenomenon. A somewhat more general approach is to consider two-parameter delamination shapes, such as ellipses, e.g. Chai[8] and Yin and Jane[9]. It is obvious though that delaminations might have arbitrary shape and any assumption regarding the shape of the delamination might lead to misleading conclusions.

The earliest computational result for the energy release rate in more general situations are due to Whitcomb[10], who computed the energy release rate for an embedded circular delamination loaded in uniaxial compression by aid of a three-dimensional finite element formulation and the crack closure method. Storåkers and Andersson[11] pursued a different approach and developed a method to compute the energy release rate at *local* crack growth within von Karman's nonlinear plate theory. Their resulting expression was a simple algebraic one involving only plate resultants along the crack front. Nilsson and Giannakopoulos[12] implemented this

Copyright © 1994 by ICAS and AIAA. All rights reserved.

method into a FE-code and extended it with a method to automatically update the FE-mesh. This allowed them to simulate delamination growth without any bias regarding the shape of the delamination. This method was later extended to include the effect of friction-free contact between delaminated members at buckling as well as at postbuckling, Giannakopoulos *et al.*[13]. In order to assess the applicability of their model a combined theoretical/ numerical and experimental analysis was undertaken for initially circular and embedded delaminations in layered carbon-reinforced epoxy materials and loaded in uniaxial compression by Nilsson *et al.*[14]. Excellent agreement between measurements and computed results was observed for the shape of the delamination after growth as well as the load required to sustain crack growth.

Cracks in homogeneous and brittle materials tend to propagate such that a pure opening mode (Mode I) is sustained at the crack tip. In layered materials, cracks tend to propagate along the weaker interfaces where a mixed mode crack tip loading is generally expected. Experiments have shown that the fracture resistance in shearing and sliding (Mode II and III) might be substantially larger than in opening e.g. Sela and Ishai[15] for composites and [4] for coating materials used in electronic industry. This elucidates the importance of separating the crack driving force into fracture modes in the analysis. Whitcomb[10] realized the significance of separating the fracture modes already in his earliest works and where the energy release rate was decomposed into the three fundamental fracture modes. It should be emphasized that the fracture mode decomposition depends on the local crack tip loading and attempts to separate the fracture modes based on simple beam or plate theories such as suggested in[16] will in most cases not give even qualitatively acceptable results. Suo and Hutchinson[17] were able to decompose the fracture modes as function of the load resultants for an isotropic split beam element by an integral equation formulation. Nilsson and Storåkers[18] later showed in general circumstances that the nonlinear plate problem locally can be reduced to an equivalent 2-D split beam problem. By this procedure the mode decomposition may be achieved by identification with the split beam problem.

This paper gives an overview on a method to compute the stress intensity factors and the energy release rate at local crack growth for quite general crack fronts and loadings. The technique is then used in conjunction with a moving boundary technique to simulate delamination growth and where no biassed assumptions are made regarding the shape of the delamination front. The technique will be illustrated with several examples and comparison with experiments are also given.

THEORY AND NUMERICAL PROCEDURE

To model the structure depicted in Fig. 1 a non-linear Mindlin plate theory seems appropriate to account for the deflection of thin bodies at small strains but at moderate rotations. The displacement field is then given by

$$\left.\begin{aligned} u_\alpha(x_i) &= \bar{u}_\alpha(x_\beta) + x_3\theta_\alpha(x_\beta) \\ u_3(x_i) &= \bar{u}_3(x_\beta) \end{aligned}\right\} \qquad (1)$$

where Greek and Roman indices run from 1 to 2 and 1 to 3 respectively. θ_α denotes the rotation of a transverse material fibre and barred displacements refer to the mid-plane. Indices 1 and 2 refer to in-plane quantities and 3 to the normal direction. The small strain tensor components become

$$\begin{aligned} e_{\alpha\beta} &= e^0_{\alpha\beta} + x_3\kappa_{\alpha\beta} \\ e_{3\alpha} &= (\bar{u}_{3,\alpha} + \theta_\alpha)/2 \end{aligned} \qquad (2)$$

where the stretching of the middle surface, $e^0_{\alpha\beta}$, is $(\bar{u}_{\alpha,\beta} + \bar{u}_{\beta,\alpha} + \bar{u}_{3,\alpha\beta})/2$, the curvature, $\kappa_{\alpha\beta}$, is $(\theta_{\alpha,\beta} + \theta_{\beta,\alpha})/2$, and $e_{3\alpha} = e_{\alpha 3}$ is the transverse shear. The material is assumed to be linearly elastic and the conjugate forces generated by the strain energy function W are

$$N_{\alpha\beta} = \frac{\partial W}{\partial e^0_{\alpha\beta}},\ 2Q_\alpha = \frac{\partial W}{\partial e_{3\alpha}},\ M_{\alpha\beta} = \frac{\partial W}{\partial \kappa_{\alpha\beta}}. \qquad (3)$$

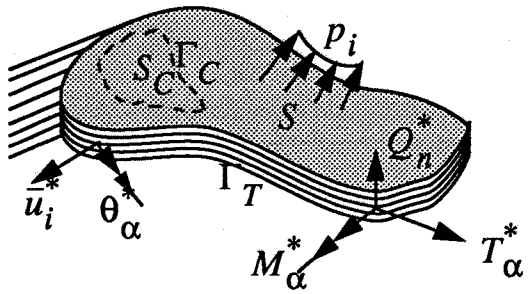

Fig.2 Multilayered composite plate with a plane crack parallel to an interface

The resulting governing equations and dynamic boundary equations are readily derived by the principle of virtual work

$$\left.\begin{aligned} N_{\alpha\beta,\beta} + p_\alpha &= 0 \\ M_{\alpha\beta,\beta} - Q_\alpha &= 0 \\ Q_{\alpha,\alpha} + N_{\alpha\beta}n_\alpha\bar{u}_{3,\beta} \end{aligned}\right\} \qquad (4)$$

and

$$\left.\begin{aligned} N_{\alpha\beta}n_\beta &= T^*_\alpha \\ M_{\alpha\beta}n_\beta &= M^*_\alpha\varepsilon_{\alpha\beta} \\ Q_\alpha n_\alpha + N_{\alpha\beta}n_\alpha\bar{u}_{3,\beta} &= Q^*_n \end{aligned}\right\} \qquad (5)$$

with notations shown in Fig. 2, and $\varepsilon_{\alpha\beta}$ being the two-dimensional permutation tensor. These equations constitute a standard boundary value problem to be solved by the finite element code ADINA.

It has been observed that delaminated members, as at issue here, often tend to interpenetrate each other if unconstrained. Such interpenetration is physically unacceptable, instead the members will be in contact. The contact area is, however, not equal to the penetration area and moreover it also changes with the load. A contact finite element procedure consistent with the present nonlinear plate theory was therefore developed and used in conjunction with the finite element code[13]. A predictor-corrector procedure is used to compute the contact area. The procedure is straight-forward and based on controlling the transverse displacements and reaction forces in the contact area, Ω_C, as illustrated in Fig. 3.

$$\left.\begin{aligned} &\bar{u}_3(x_1, x_2) = 0, \bar{u}_{3,\alpha}(x_1, x_2) = 0 \\ &R_N(x_1, x_2) > 0 \end{aligned}\right\} \qquad (6)$$

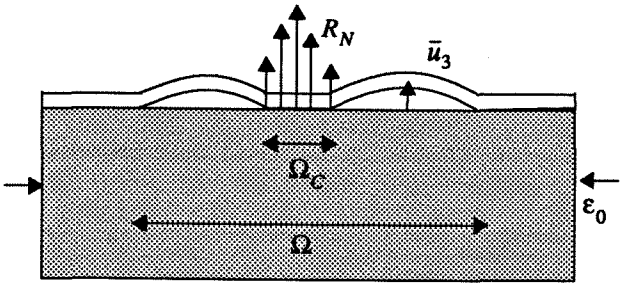

Fig. 3 One-dimensional illustration of contact at delamination

The contact region is assumed to be computed with sufficient accuracy when

$$1 - \frac{\int_\Omega \bar{u}_3(x_1, x_2)\, d\Omega}{\int_\Omega |\bar{u}_3(x_1, x_2)|\, d\Omega} < \varepsilon \qquad (7)$$

where ε is a convergence norm. When contact occurs already at buckling, the iterative procedure to compute the contact area requires particular providence as detailed in [13] and [14].

Storåkers and Andersson[11] showed that the energy release rate at local crack extension within von Karman's nonlinear formulation can be expressed as the discontinuity across the crack front of an energy momentum tensor expressed in the plate variables.

$$G = \| P_{\alpha\beta} \| \qquad (8)$$

where the double brackets denotes the "jump". The equivalent expression within the present shear deformable theory for the energy momentum tensor, $P_{\alpha\beta}$, is[14]

$$W\delta_{\alpha\beta} - N_{\alpha\beta}\bar{u}_{\gamma,\beta} - Q_\alpha \bar{u}_{3,\beta} - M_{\alpha\gamma}\theta_{\gamma,\beta}. \qquad (9)$$

The algebraic expression defined by Eqns (8) and (9) is readily implemented into any standard nonlinear finite element code. In the von Karman formulation the contribution to the energy release from the transverse shear component vanishes and $\theta_{\gamma,\beta}$ is replaced by $-\bar{u}_{3,\gamma\beta}$.

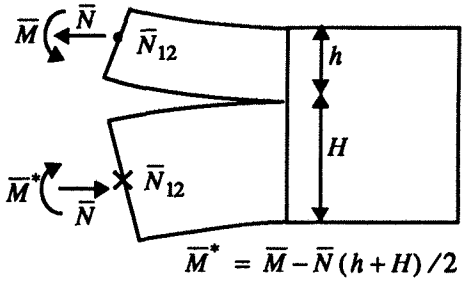

Fig. 4 Loaded split beam element after superposition.

The significance of decomposing the crack driving force into the fundamental fracture modes was mentioned in the introduction. For an isotropic split beam with loading as shown in Fig. 4, Suo and Hutchinson [17] determined the stress intensity factors as

$$\begin{aligned} K_I &= \frac{1}{\sqrt{2t}}\left(-N\cos\omega - \sqrt{12}\frac{M}{t}\sin\omega\right) \\ K_{II} &= \frac{1}{\sqrt{2t}}\left(-N\sin\omega + \sqrt{12}\frac{M}{t}\cos\omega\right) \end{aligned} \qquad (10)$$

where $\omega = 52.1°$ for an isotropic and homogenous material. The energy release rate is uniquely associated with the stress intensity factors and in particular for an isotropic material

$$G = \frac{(1-\nu^2)}{E}\left(K_I^2 + K_{II}^2 + \frac{K_{III}^2}{1-\nu}\right) \qquad (11)$$

Suo[19] has given expressions corresponding to (10) for some anisotropic materials. For bimaterials, the singular stress field at the crack tip has an oscillatory behaviour and the conventional stress intensity cannot be defined. The nonlinear von Karman plate problem can locally at the crack tip be reduced to a split beam problem with an additional shear force as proved in[18]. For isotropic materials it also follows that the shear force component, N_{12}, only gives rise to the shearing mode (mode III)

$$K_{III} = N_{12}/\sqrt{t} \qquad (12)$$

It follows immediately that Eq (11) with (10) and (12) is identical to Eq. (8) evaluated within the von Karman plate theory.

A crack growth criterion for brittle materials loaded in mixed mode can be defined in a general form

$$f(K_I, K_{II}, K_{III}) = 0 \qquad (13)$$

to be given for a specific material.

One particular two parameter form of (13) suggested by Hutchinson and Suo[4] and which has proved to fit experimental data successfully is

$$G = G_C [1 + (\tan (1 - \lambda) \psi)^2] \qquad (14)$$

where ψ = atan (K_{II}/K_I), the phase angle, is a measure of the mode mixity and λ is a measure of the mode dependence in the crack growth criterion. The material parameters G_C and λ are determined by experiments. In the limit $\lambda = 1$ and 0, (14) corresponds to the mode insensitive criterion, $G = G_C$ and a criterion based on a critical value of K_I respectively. Experiments on epoxy/steel and epoxy/glass interface toughness show that for these materials the fracture toughness can be reasonably well characterized by (14) using $\lambda \approx 0.3$ [4].

EXAMPLES

An embedded circular blister loaded in uniaxial compression

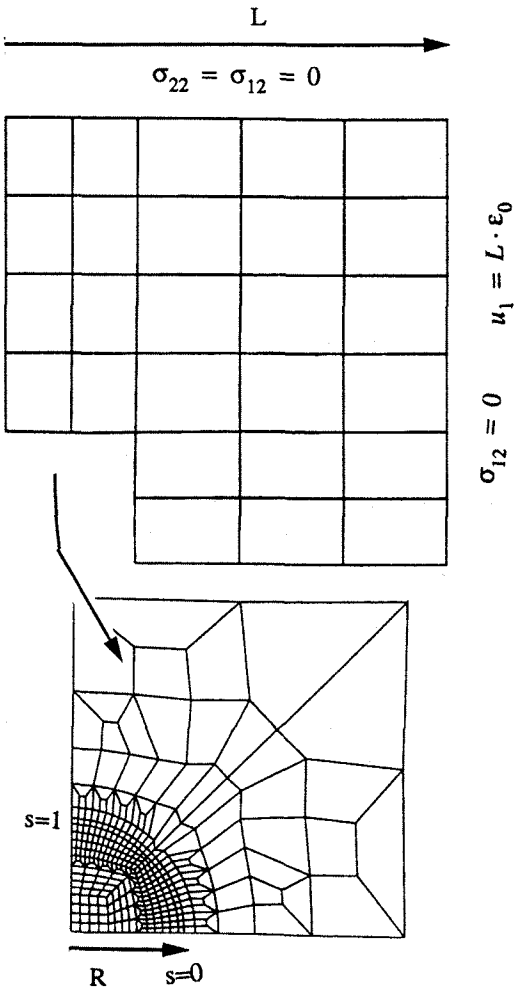

Fig. 5. The finite element mesh used in the numerical simulation together with boundary conditions.

A thin circular delamination embedded in an isotropic material and subjected to a uniaxial compression is perhaps the simplest example for which self-similar crack growth is not expected. The so called "thin film assumption", i.e. only the delaminated member will undergo bending, has proved to be very accurate for thickness ratio less than one tenth [20] ($h/H < 0.1$ in Fig. 4) and it simplifies the finite element procedure considerably. Many relevant technical problems such as coatings can essentially be regarded as thin film problems. The thin-film assumption will be adopted in the examples given in this paper.

A typical finite element mesh used in the computation is showed in Fig. 5. The elements are four-noded shell elements allowing for transverse shear and large rotations as assumed in the derivation of the equations in the previous section. The delamination front was clamped with hard conditions, i.e. giving the constraint $\bar{u}_3(x_\alpha) = 0$, $\theta_\alpha = 0$ for $x \in s$, $(0 \le s \le 1)$

We begin by analysing an isotropic material with Young's modulus, E, and Poisson's number, ν, equal to *70GPa* and *0.33* respectively and with the thickness to the radius ratio (R/t) of the delamination equal to 20.

The delamination buckles, as depicted in Fig. 1b, without being in contact with the substrate for this particular configuration at the strain load $\varepsilon_0 = \varepsilon_{buck}$, equal to $2.52\,(t/a)^2$. The delaminated plate will be in contact with the substrate when the compressive load exceeds $1.6\varepsilon_{buck}$. The contact is limited to a relatively small area along the crack front normal to the loading direction.

The stress intensity factors as function of the loading along the crack front in the post-buckled state are computed by first superposing a homogenous strain field locally at the crack tip which results in a loading situation as depicted in Fig. 4 and by subsequently applying Eq. (10) and (12) on these resultants.

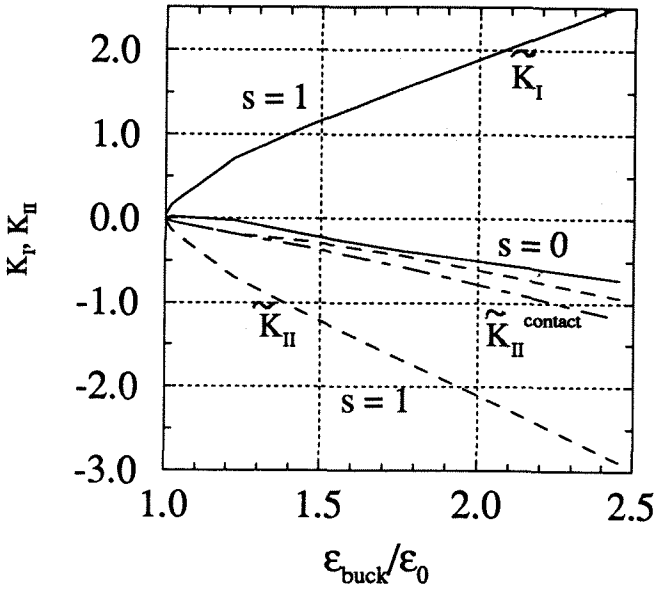

Fig. 6: Dimensionless stress intensity factors, $\tilde{K}_I$ and $\tilde{K}_{II}$ defined by $K_{I,II} = (1-\nu^2)/(E\sqrt{t})\,(R/t)^2 K_I, K_{II}$ normal (s=0) and transverse (s=1) to the loading direction as function of the normalized load $\varepsilon_0/\varepsilon_{buck}$.

Fig. 6 depicts the normalized stress intensity factors, $\tilde{K}_I$ and $\tilde{K}_{II}$, normal and transverse to the loading and as function of the compressive load, $\varepsilon_0/\varepsilon_{buck}$. It is apparent from Fig. 6 that the stress intensity factors are considerably larger in the direction transverse to the load. Another interesting feature is that the mode I stress intensity factor normal to the loading reaches a maximum at $1.1\varepsilon_0^{cr}$ and then decreases such that it becomes negative for loads exceeding $1.2\varepsilon_0^{cr}$. This indicates a *local* contact at the crack tip which precedes the *global* contact defined by Eq. (6). Local contact cannot be accepted on physical grounds. This implies that K_I is zero when the mode separation (10) results in a negative opening mode. Conservation of energy then states that the associated energy instead should be attributed to the shearing mode[13], such that

$$K_{II}^{Contact} = \sqrt{K_{II}^2 + K_I^2} \qquad \text{when} \qquad K_I < 0 \quad (14).$$

where K_{II} and K_I are evaluated in accordance with Eq. (10). The contact adjusted stress intensity factor, $K_{II}^{Contact}$, is displayed in Fig. 6 along with the stress intensity factors evaluated according to (10). The procedure embodied in (14) will be retained in remaining of this paper.

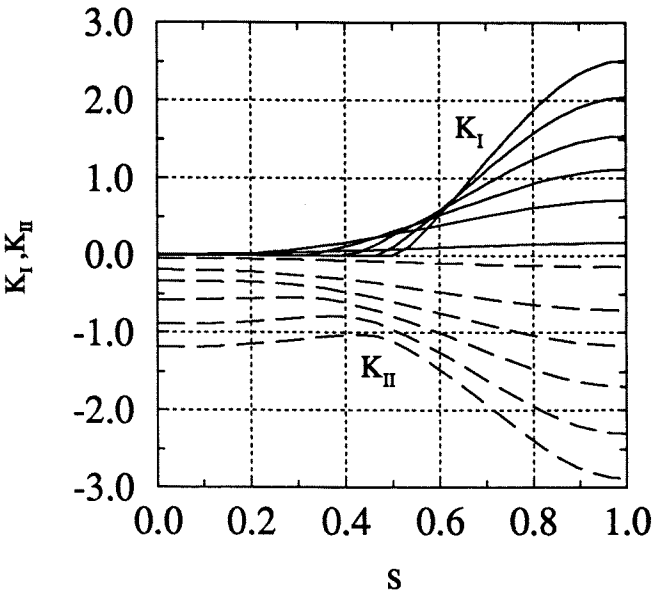

Fig. 7: Dimensionless stress intensity factors, $\tilde{K}_I$ and $\tilde{K}_{II}$ along the crack front for the load levels $\varepsilon_0/\varepsilon_0^{cr}$ = 1.05, 1.22, 1.47, 1.76. 2.11 and 2.45.

Fig. 7 shows the stress intensity factors along the delamination front for the compressive load levels $\varepsilon/\varepsilon_0^{cr}$ = 1.02 to 2.45 respectively. Both stress intensity factors attain their maximum transverse to the loading direction and crack growth is expected in this to be initiated in this direction.

The mode III stress intensity factor was found to be substantially smaller than the load resultants and stress intensity factors for mode I and II and is therefore not shown. The energy release rate associated with the transverse shear in (8) was limited to a couple percent of the total energy release rate.

Simulation of delamination growth

If we employ a crack growth criterion of the type (13), it is obvious from the stress intensity distribution displayed in Figures 6 and 7 that incipient crack growth will be in the direction transverse to the loading. The change in the delamination front will induce a redistribution of the crack growth parameters at subsequent growth. Continued growth can be analysed by the finite element method if we continuously updates the mesh as the delamination front progresses. A method to automatically update the FE-mesh and with the accuracy of the numerical results retained is therefore an essential ingredient in a growth simulation. Such a method, based on minimizing the total change in element angles for a prescribed change of boundaries is described in[12] and is adopted in the examples below.

The simulation for quasi-static buckling-driven delamination growth with a growth criterion of the type (13) can be summarized as follows: i) the buckling load for the present load and configuration is computed; ii) this is followed by a postbuckling analysis where the crack growth parameters are computed as function of the load along the crack front. The load increments are chosen such that the crack growth criterion is attained at some part along the crack front in relatively few postbuckling steps. Load increments should not jeopardize the numerical stability and the crack growth criterion should not be to much exceeded: iii) nodes along the crack front that have attained the crack growth criterion are being propagated in the direction normal to the present crack front by a used-defined crack increment, Δa; iv) the automatic mesh generator mentioned above then updates the mesh in accordance with the new front.

A simulation of quasi-static delamination growth with a continuously modified delamination front can then be simulated by repeating the steps i-iv an many times as needed. The relevant results as the crack advances are: the delamination front; the load required to sustain growth; and the distribution of crack growth parameters at growth.

Choosing the user defined crack increment, Δa, too small will make the growth process slow, on the other hand a large value will induce oscillations in the distribution of the crack growth parameter along the propagating part of the front which will retard the process. Numerical experiments indicate that choosing Δa to be approximately 0.5 to 1% of a typical length of the delamination is a reasonable compromise.

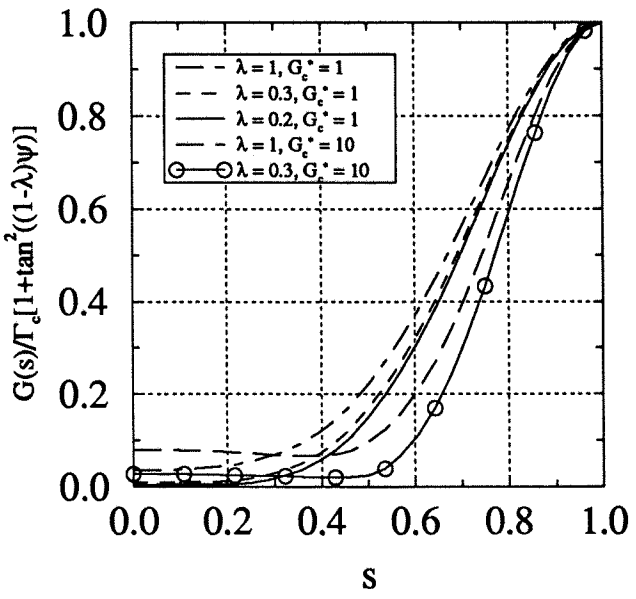

Fig 8: Normalized G-distributions at crack growth initiation for the five combinations, $(\lambda = 1, \tilde{G}_c = 1)$, $(\lambda = 0.3, \tilde{G}_c = 1)$, $(\lambda = 0.2, \tilde{G}_c = 1)$, $(\lambda = 1, \tilde{G}_c = 10)$, $(\lambda = 0.3, \tilde{G}_c = 10)$, *where* $\tilde{G}_c = (R/t)^4 (1-\nu^2)/(Et)$

Fig.8 shows the G-distribution at the applied growth loads given in Table 1. Each curve represents a particular combination of λ and $\tilde{G}_c$ of the mixed mode criterion (14) as detailed in the Figure text and in Table 1. The energy release rates are normalized with the crack growth criterion. We note that the peak in the distribution at s = 1, i.e transverse to the loading direction, tends to be more pronounced as the mode II toughness increases.,

Table 1: *The normalized load,* $\varepsilon_o/\varepsilon_{buck}$ *required to initiate crack growth for a circular delamination loaded in uniaxial compression.* $\varepsilon_{buck} = 2.52\,(t/R)^2$

	$\lambda = 1$	$\lambda = 0.3$	$\lambda = 0.2$
$\tilde{G}_C = 1$	1.221	1.286	1.311
$\tilde{G}_C = 10$	2.137	2.427	----------

Fig. 9 a-e display the evolution of the crack fronts for the five parameter combinations. The shape of the crack front depends clearly on the adopted crack growth criterion. As already pointed out for the distribution of the crack growth parameter, increasing mode dependence and increasing fracture toughness increase the localization of the growth. The shapes illustrated in 9a-d seem to be almost elliptical. The last case, $\lambda = 0.3$ and $\tilde{G}_c = 10$, clearly deviates from the elliptical shape after growth.

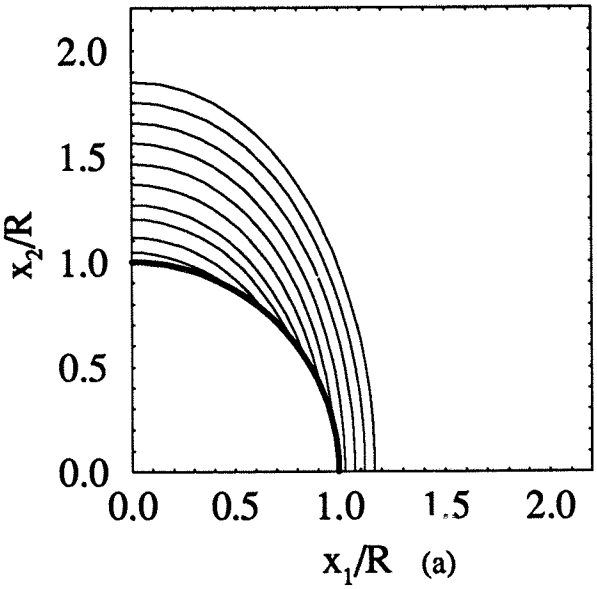

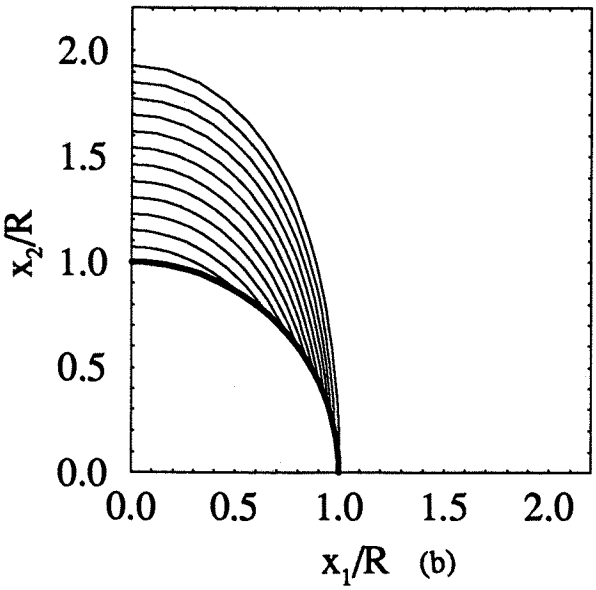

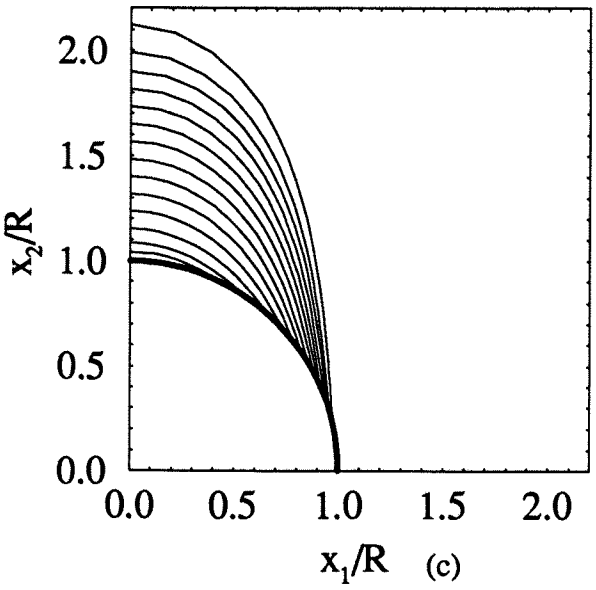

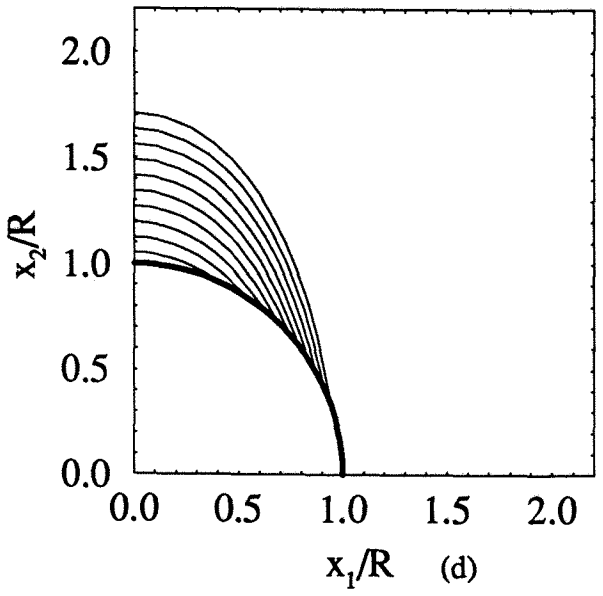

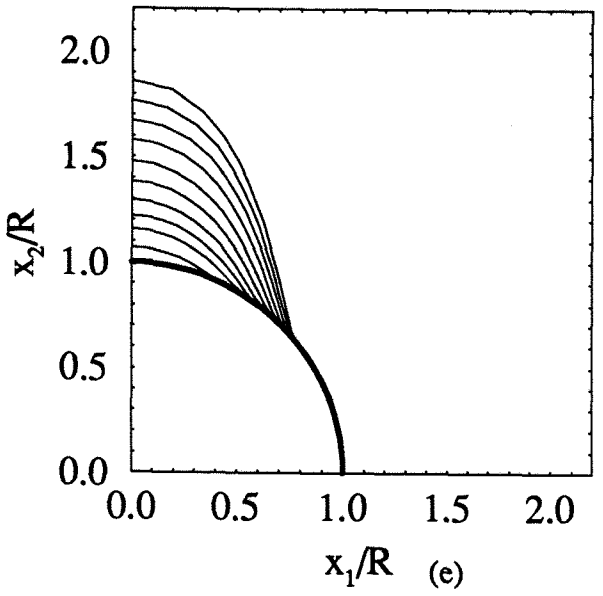

Fig. 9: Successive crack fronts
(a) ($\lambda = 1, G_c = 1$) *(b)* ($\lambda = 0.3, \tilde{G}_c = 1$)
(c) ($\lambda = 0.2, G_c = 1$) *(d)* ($\lambda = 1, G_c = 10$)
(e) ($\lambda = 0.3, G_c = 10$)

The number of crack increments employed to compute the final shape in 9a-e ranged from 100 to 250.
The phase angle, ψ, transverse to load varied from 45.3 to 48.7 for the five cases at initial growth, and hence the K_I/K_{II} ratio was close to unity. Although the shapes differ from each other this ratio was also approximately retained as the delamination was spreading. The phase angle at *s=1* for the last front depicted in Fig. 9a-e was within 47.0- 48.1 degrees.

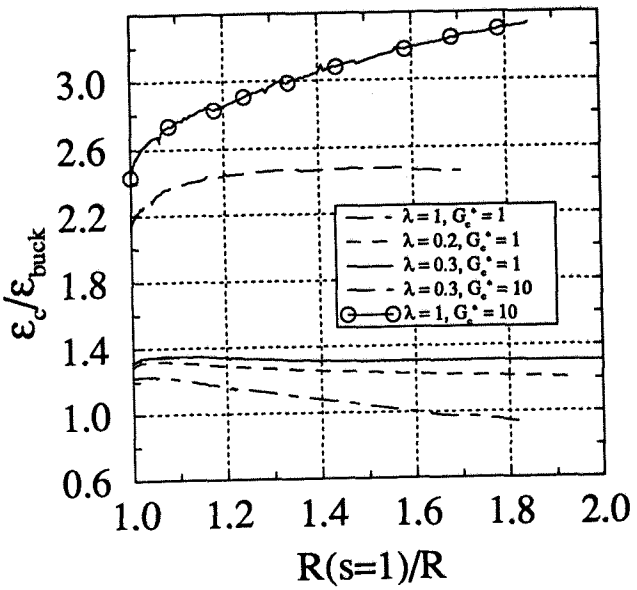

Fig. 10: Compressive normalized strain required to sustain growth as function of growth in the transverse direction for the shapes in Fig. 9a - 9e.

From a structural point of view, the stability of the growth is far more relevant than the shape. The curves in Fig. 10 show the load required to sustain growth, ε_c, for the five crack growth parameter combinations given Table 1. An increasing load as the crack advances implies stable growth whereas a decreasing load implies unstable growth.
By comparing the stability feature in Fig. 10 with the normalized G-distribution we note a correlation between more pronounced localization in the distribution of the crack growth parameters and an increased tendency for stable growth. This observation suggests that it might be sufficient, at least for a qualitative assessment of the crack growth stability of incipient growth, to study the initial crack growth distribution.

A combined numerical/theoretical and experimental investigation of interface crack growth.

A combined experimental and numerical/theoretical investigation was carried out to assess the applicability of the proposed method for analysis of delamination growth[14]. It was decided that the specimen should be designed so that the expected delamination growth should be stable and localized. In addition to these criteria, the specimen should fit into an existing anti-buckling frame which preserves the global stability of the plate specimen.

Experimental Procedure

The material used in the experiments was Ciba-Geigy epoxy carbon prepeg 6376/HTA7 of nominal ply thick-

ness of 0.127 mm and with the elastic ply properties E_{11}=145.6GPa, E_{22}=10.5GPa, G_{12}=5.25GPa, ν_{12}=0.3. The complete three-dimensional properties were determined under the following common assumptions: $G_{13}=G_{12}$, ν_{23}=0.51 and $G_{23}=E_{22}/[2(1+\nu_{23})]$. The specific Mode I and Mode II data for the energy release rate were 196 and 596 Jm^{-2} respectively as shown in Fig. 11

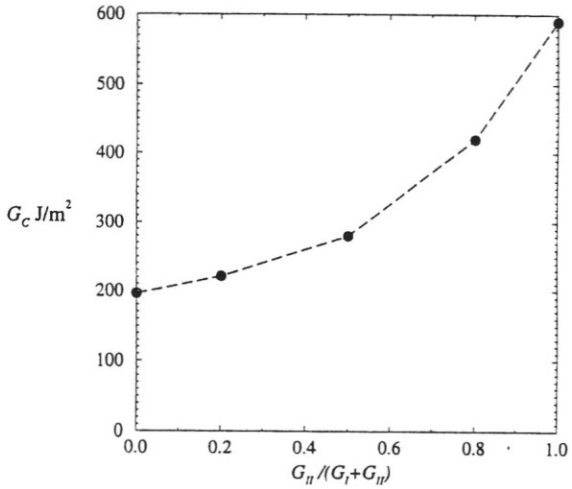

Fig. 11: Measured fracture toughness as a function of the mode mixity for a unidirectional layup of carbon/epoxy 6376C/HTA7 (From [14])

A cross-ply layup $(90/0/90)_{16}$ was chosen for the experimental setup with the ply orientation measured from the loading direction. A circular delamination was introduced between the third and fourth plies. The 90-plies served to preserve maximum stiffness in the transverse load direction, which according to preliminary computations would result in stable and localized growth. The cross-ply of the lay-up needed to prevent the crack from kinking out-of-plane and the prerequisite that the delamination should propagate between equally orientated plies required three layers above the delamination. The thickness ratio between the delaminated plies and the total specimen (1/16) was assumed sufficient to motivate the thin-film assumption.

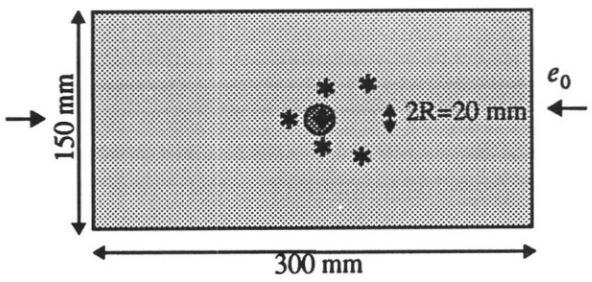

Fig. 12 Specimen geometry for plates and strain gauge layout used in the experiments. Gauges on front face ✱ and ✚

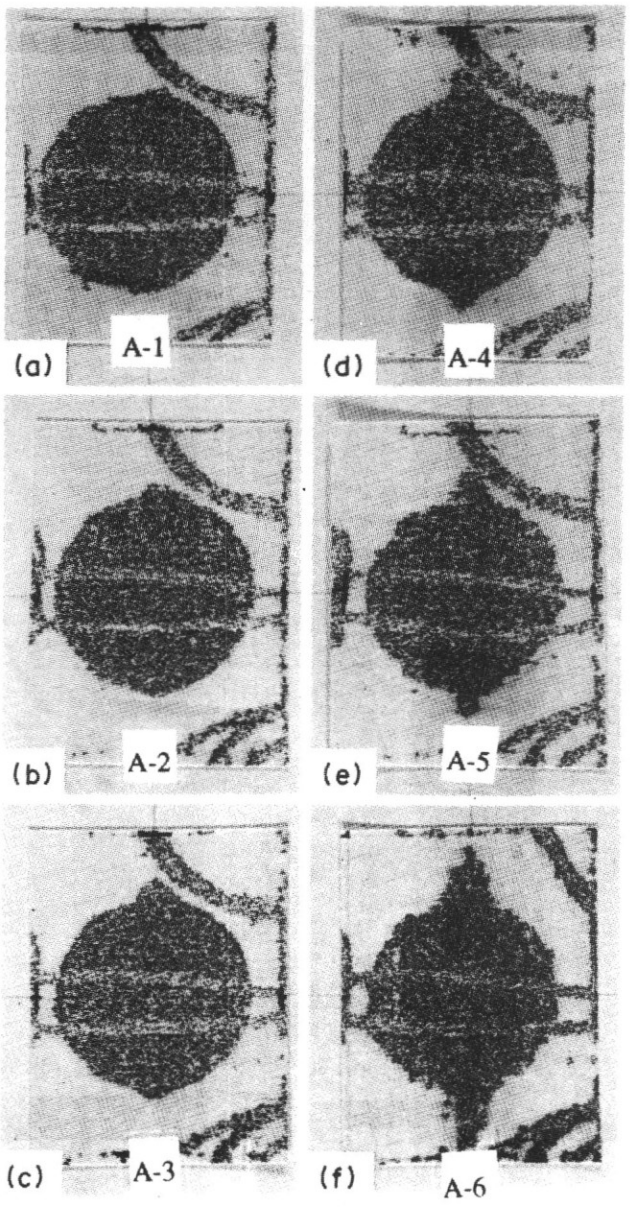

Fig. 13: Successive delamination shapes at six strain load levels as given by the C-scan technique. (From [14])

Five strain gauges were attached to the specimen in order to measure the in-plane strain field and an additional one to verify that global bending of the panel was small. The geometry of the specimen together with the approximate positioning of the strain gauges is shown in Fig. 12. Acoustic emission technique was employed to determine the buckling load. The initiation of each crack increment and ultrasonic C-scan and occasionally X-ray technique was adopted to map the crack fronts. Three nominally identical specimens were tested. The in-plane strain field was continuously measured and the compressive load was slowly increased until the delaminated plate buckled. The load was further increased until crack growth was recorded. At this point the test was arrested. The specimen was dismounted and the extent of delamination growth was mapped. The specimen was then remounted and the procedure repeated.

Growth was stable and in the transverse load direction. The measured buckling strain was 2.2×10^{-3}, 2.2×10^{-3}, 2.1×10^{-3} and the load at initial delamination growth was 3.3×10^{-3}, 3.4×10^{-3}, 3.2×10^{-3}. The successive shapes for one of the specimens is shown in Fig. 13. The growth pattern was similar for the other specimens. A more detailed description on the experimental procedure is given in [14] or [21].

Numerical Simulation

The numerical procedure described earlier was employed to simulate the experiments. Standard laminate theory was used to determine the membrane and bending stiffness with the particular layup taken into account. Shear factors in the spirit of Reissner were adopted in the constitutive law to compensate for the additional stiffness resulting from constant transverse shear strain. The mesh was similar to the one depicted in Fig. 5, except that the meshing was slightly denser in the transverse load direction.

The experiments showed that crack growth was initiated at $\varepsilon_0 = 3.3 \times 10^{-3}$. The computed G-distribution at this load is depicted in Fig. 14, and as expected the largest value appears transversely to the loading (s=1). The computed energy release rate at this specific load level was *217 Jm^{-2}*, which can be compared with the mode dependant critical values plotted in Fig. 11. The energy release rate associated with transverse shear accounts for approximately 10% of the total energy release rate. The fracture mode decomposition defined by Eq. (10) and (14) does not apply strictly for this material combination. An *ad hoc* decomposition could be adopted, however, its validity can be questioned. We note from Fig. 11 that the mode dependence is relatively weak when $G_{II}/(G_I + G_{II}) < 0.5$. It was mentioned for the isotropic cases above that the mixed mode ratio was very close to unity at the point transverse to the load direction. It is also worth pointing out that the critical crack growth parameters were only known for crack fronts orthogonal to fibres. Due to these uncertainties it was found advisable to adopt the growth criterion $G=G_c$, with $G_c=217\,Jm^{-2}$ at initiation as well as continued growth.

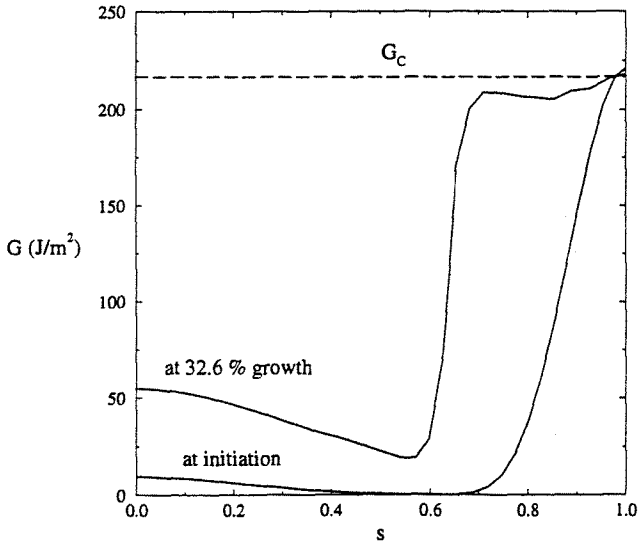

Fig. 14: The energy release rate distribution for the initially circular front and for the front after 32.6% growth.(From [14])

Contact occurred already at buckling for this configuration. The buckling load without contact was 1.9×10^{-3} whereas the buckling analysis with contact gave a buckling strain of 2.12×10^{-3} which is in excellent agreement with the measured values given above.

Fig. 15 shows five crack fronts with associated compressive loads and we note that the fronts seem to correspond well with the measured fronts in Fig. 13.

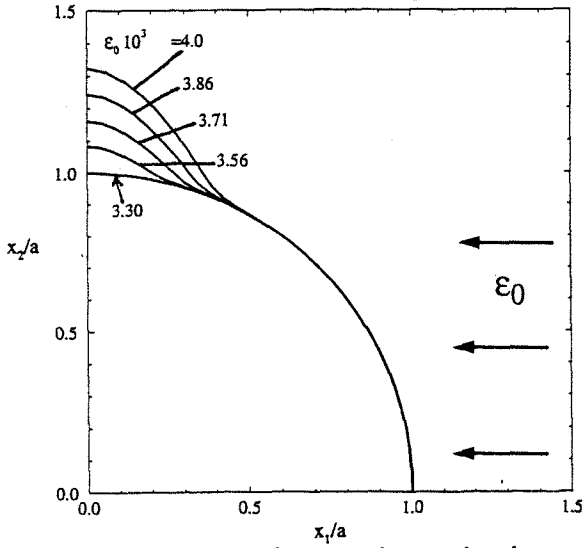

Fig. 15: Successive crack fronts with associated compressive load.(From [14])

The close agreement between computed and measured fronts become even more striking when they are shown together as in Fig. 16.

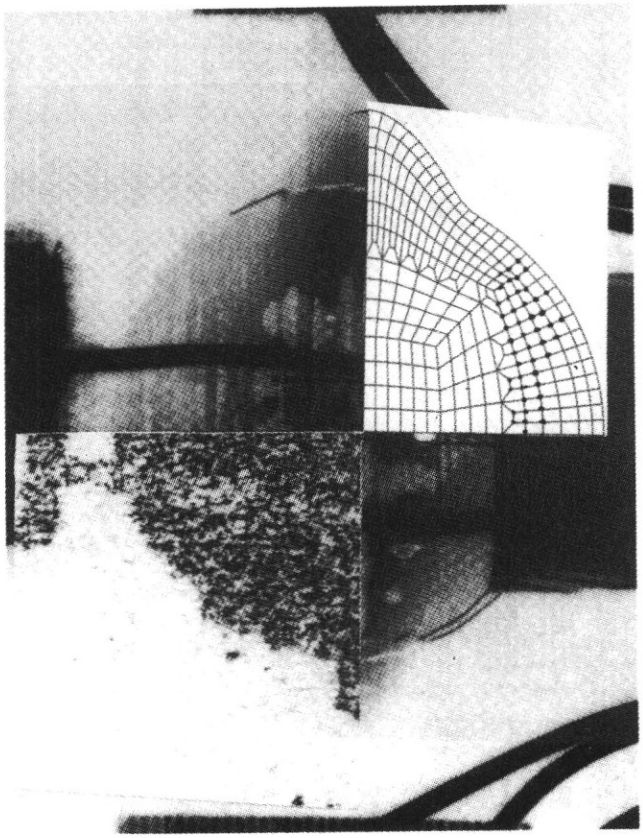

Fig. 16: The delamination front as given by X-radiography with C-scan and the corresponding FE-mesh with nodes in contact depicted. (From [14])

The G-distribution for this front is shown in Fig. 14 along with the initial one. The computed compressive load required to sustain growth as function of the growth in the transverse direction is shown in Fig. 17 together with the measured values for each of the two advancing fronts. It is remarkable how well the computed and experimental growth resistance correspond for this configuration. The mesh for the initially circular and the final shape corresponding to 32.6% growth are shown with nodes in contact in Fig. 18. The quality of the mesh has been relatively well retained by the successive updating of the mesh. We also note that the contact region has shifted slightly during growth.

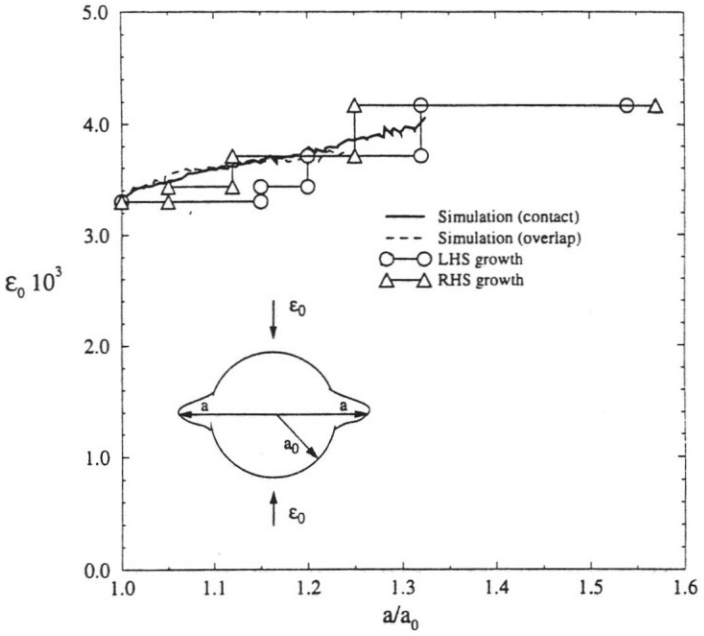

Fig: 17 Compressive load required to sustain growth. (From [14])

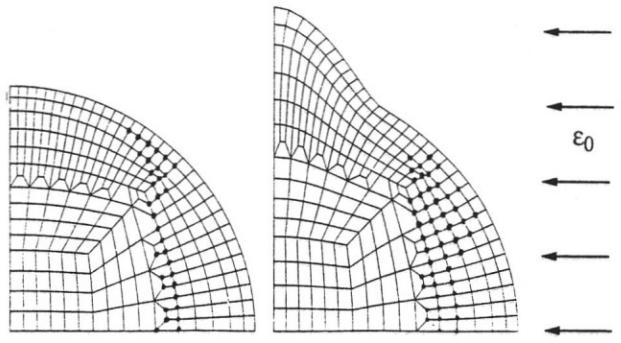

Fig. 18: The FE-Mesh with nodes in contact at initial growth and at 32.6% growth. (From [14])

CONCLUDING REMARKS

A theoretical/numerical model to analyse buckling-driven delamination growth has been presented. Expressions for the energy release rate and stress intensity factors at local crack growth within kinematically nonlinear plate theories are given. In conjunction with an automatic mesh generator it was then possible to analyse delamination growth at arbitrary crack shapes. Predicted results were compared with observed ones in a combined numerical/experimental investigation of a single embed-

ded delamination in a carbon epoxy laminate loaded in uniaxial compression. The predicted results captured the observed shapes of the delamination after growth as well as the load needed to sustain growth. In order to assess the general applicability other material combinations and loadings should be analysed in combined experimental/ numerical studies similar to the one described here. Based on the excellent reproducibility of the test results, it is believed that the proposed method will be a useful tool to analyse interface crack growth in a variety of situations.

REFERENCES

[1] Garg, A.C., 1988, "Delamination- A Damage Mode in Composite Structures", Engineering Fracture Mechanics, **29**, 557-584.

[2] Storåkers B.,1989, "Nonlinear aspects of delamination in structural members", *Proceedings of the 17th International Congress of Theoretical and Applied Mechanics*, (Eds Germain, P., Piau, M., and Caillerie, D.), pp. 689-718

[3] Abrate, S., 1991, "Impact on laminated composite materials", *Applied Mechanics Reviews*, **44**, No. 4, pp. 155-190.

[4] Hutchinson, J. W., and Suo, Z., 1991, "Mixed mode cracking in layered materials", *Advances in Applied Mechanics*, **29**, pp 63-191.

[5] Kachanov, L.M., 1976, "Separation failure of composite materials", *Mekhanika Polimerov* (English translation), **5**, pp. 918-922.

[6] Chai, H., Babcock, C.D. and Knauss, W.G., 1981, "One Dimensional Modeling of Failure in Laminated Plates by Delamination Buckling", *International Journal of Solids and Structures*, **17**, pp. 1069-1083.

[7] Yin, W.L., 1985, "Axisymmetric Buckling and Growth of a Circular Delamination in a Compressed Laminate", *International Journal of Solids and Structures*,.**21**, pp. 503-514.

[8] Chai, H. and Babcock, C.D., 1985, "Two-dimensional modelling of compressive failure in delaminated plates", *Journal of Composite Materials*, **19**, pp. 67-96.

[9] Yin, W.-L., and Jane, K.C., 1991, "Refined buckling and postbuckling analysis of two-dimensional delaminations-I. Analysis and Validation", *International Journal of Solids and Structures*, **29**, pp. 591-610.

[10] Whitcomb J.D. (1986) "Parametric Analytical Study of Instability-Related Delamination Growth", Composite Science and Technology, 25, pp 19-48.

[11] Storåkers, B. and Andersson, B., 1989, "Nonlinear plate theory applied to delamination in composites", *Journal of the Mechanics and Physics of Solids*,. **36**, pp. 689-718

[12] Nilsson, K.-F., and Giannakopoulos, A.E., 1990, "Finite Element Simulation of Delamination Growth", *Proceedings of the first International Conference on Computer-Aided Assessment and Control of Localized Damage*, (Eds Aliabadi, M.H., Brebbia, C.A., and Cartwright, D.J), pp. 299-313.

[13] Giannakopoulos, A.E, Tsamasphyros, G. and Nilsson, K.-F., *The contact problem in delamination, Report 137* Department of Solid Mechanics, Royal Ins. of Technology, Stockholm, Sweden.

[14] Nilsson, K.-F., Thesken, J.C., Sindelar, P., Giannakopoulos and Storåkers, B. (1993) "A Theoretical and Experimental Investigation of Buckling Induced Delamination Growth, *Journal of the Mechanics and Physics of Solids*, **41**, pp. 749-782.

[15] Sela, N., and Ishai, O., 1989, "Interlaminar fracture toughness and toughening of composite materials: a review", *Composites*, Vol. 20, No. 5, pp. 423-435.

[16] Williams, J.G., 1988, "On the calculation of energy release rates for cracked laminates", *International Journal of Fracture*, **36**, pp. 101-119.

[17] Suo, Z. and Hutchinson, J.W., 1990, "Interface crack between two elastic layers", *International Journal of Fracture*, **43**, pp. 1-18.

[18] Nilsson, K.-F., and Storåkers, B., 1992, "On Interface Crack Growth in Composite Plates", *Journal of Applied Mechanics, 59, pp 530-538.*

[19] Suo, Z., 1990, "Delamination specimens for orthotropic materials", *Journal of Applied Mechanics*, **43**, pp. 627-634.

[20] Larsson, P.-L. (1991) "On Delamination Buckling and Growth in Circular and Annular Orthotropic Plates", International Journal of Solids and Structures, **27**, pp 15-28.

[21] Thesken, J.C., 1994 "Investigations of Delamination Growth Rate and Criticality Along Heterogeneous Interfaces", *Proceedings 19th Congress of the International Council of the Aeronautical Sciences.*